

Review

Recent Advances in Ternary Metal Oxides Modified by N Atom for Photocatalysis

Jingwen Wang¹, Takuya Hasegawa¹, Yusuke Asakura² and Shu Yin^{1,3,*}

¹ Institute of Multidisciplinary Research for Advanced Materials (IMRAM), Tohoku University, 2-1-1, Katahira, Aoba-ku, Sendai 980-0877, Japan

² Kagami Memorial Research Institute for Materials Science and Technology, Waseda University, 2-8-26, Nishiwaseda, Shinjuku-ku, Tokyo 169-0051, Japan

³ Advanced Institute for Materials Research (WPI-AIMR), Tohoku University, 2-1-1, Katahira, Aoba-ku, Sendai 980-0877, Japan

* Correspondence: yin.shu.b5@tohoku.ac.jp

Abstract: Ternary metal oxides (TMOs) with flexible band structures are of significant potential in the field of photocatalysis. The efficient utilization of renewable and green solar energy is of great importance to developing photocatalysts. To date, a wide range of TMOs systems has been developed as photocatalysts for water and air purification, but their practical applications in visible light-assisted chemical reactions are hindered mainly by its poor visible light absorption capacity. Introduction of N atoms into TMOs can narrow the band-gap energy to a lower value, enhance the absorption of visible light and suppress the recombination rate of photogenerated electrons and holes, thus improving the photocatalytic performance. This review summarizes the recent research on N-modified TMOs, including the influence of N doping amounts, N doping sites, and N-induced phase transformation. The introduced N greatly tuned the optical properties, electronic structure, and photocatalytic activity of the TMOs. The optimal N concentration and the influence of N doping sites are investigated. The substitutional N and interstitial N contributed differently to the band gap and electron transport. The introduced N can tune the vacancies in TMOs due to the charge compensation, which is vital for inducing different activity and selectivity. The topochemical ammonolysis process can convert TMOs to oxynitride with visible light absorption. By altering the band structures, these oxynitride materials showed enhanced photocatalytic activity. This review provides an overview of recent advances in N-doped TMOs and oxynitrides derived from TMOs as photocatalysts for environmental applications, as well as some relevant pointers for future burgeoning research development.

Keywords: ternary metal oxides; photocatalysis; N doping; oxynitrides; environmental purification



Citation: Wang, J.; Hasegawa, T.; Asakura, Y.; Yin, S. Recent Advances in Ternary Metal Oxides Modified by N Atom for Photocatalysis. *Catalysts* **2022**, *12*, 1568. <https://doi.org/10.3390/catal12121568>

Academic Editor: Edward G. Gillan

Received: 3 November 2022

Accepted: 30 November 2022

Published: 2 December 2022

Publisher's Note: MDPI stays neutral with regard to jurisdictional claims in published maps and institutional affiliations.



Copyright: © 2022 by the authors. Licensee MDPI, Basel, Switzerland. This article is an open access article distributed under the terms and conditions of the Creative Commons Attribution (CC BY) license (<https://creativecommons.org/licenses/by/4.0/>).

1. Introduction

Energy is a critical issue related to all trades and professions. Therefore, it is an indispensable factor in influencing the economy and developing modern society for the whole world. Stepping into 21st century, the sharp increasing global energy consumption leads to one of the biggest challenges, the energy crisis, because of the fast expansion of industry and growth of the world population. Under such a circumstance, one of the Sustainable Development Goals (SDGs) of the 2030 Agenda has been proposed to ensure access to affordable, reliable, sustainable, and modern energy. It is urgent and imperative to significantly limit fossil fuel consumption and explore alternatives to meet the global issue and preserve the opportunities for future generations to live in dignity and prosperity. Nowadays, various renewable and green energy, such as solar, wind, tides, waves, and geothermal heat, have been developed. Moreover, efficient utilization of renewable energy is also one of the most important issues for realizing a green and sustainable society. Solar energy is the most abundant source of renewable energy available in most parts of the world. It is necessary to capture solar energy and transform it into other usable chemical

energy that can be transported and stored. However, its technically available potential and efficiency should be improved to meet the needs of the energy supply. Besides, in the 21st century, we are confronting enormous environmental issues, including hazardous wastes, toxic heavy metals, and contaminated groundwater, which are closely related to human health. Applied solar energy to construct the environmental pollutants in air and water is a green and sustainable approach, which is beneficial for both water and energy crises. Technologies based on solar energy are also crucial for reducing carbon emissions on a global scale. However, some technical barriers, such as low efficiency, energy storage, conversion efficiency, and high cost, should be addressed and improved in the future. To this end, the development of novel and functional materials is a promising approach to apply to energy and environmental issues. Semiconductor materials have attracted considerable attention due to their versatile physicochemical properties. This material has been applied in a wide field, especially as photocatalysts. Semiconductors as photocatalysts with their unique electronic structure offer the possibility of utilizing naturally available and renewable solar energy as a light source for photochemical waste remediation, thereby making the process green and sustainable. Nowadays, extensive research is being conducted to develop and produce large-scale functional photocatalytic materials with the assistance of cutting-edge approaches to detect and eliminate hazardous contaminants in the environment.

Since water photolysis was discovered by Fujishima et al. [1] with TiO_2 as a photocatalyst for the production of O_2 and H_2 from water, many kinds of semiconductors have been fabricated and applied as photocatalysts, especially for the widely studied oxide materials. It is accepted that the properties of materials greatly changed according to their synthesis process, chemical components, morphologies, surface modification, elements doping and the formation of composites etc. [2–7]. The simple binary metal oxides or metal-free semiconductors, such as TiO_2 , ZnO , WO_3 and C_3N_4 , etc., have been widely studied as photocatalysts to understand the fundamental principle, the improvement of photocatalytic efficiency and the expansion in other potential applications [8–13]. The ternary metal oxides (designated as $\text{A}_x\text{B}_y\text{O}_z$) with more flexible band structures possess great potential to be applied as photocatalysts. A wide range of ternary metal oxides (TMOs) have been fabricated, and their photocatalytic activity related to morphology, electronic, optical properties should be further investigated. The different constituent elements in the $\text{A}_x\text{B}_y\text{O}_z$ composition provide multiple choices to modify the materials with tuning physical and chemical properties for an enhancement of photocatalytic performance.

The efficiency of the photocatalytic processes strongly depends on the properties of the photocatalysts, including (I) the surface area of the material, which influences the adsorption phenomena, and (II) the morphology of the material, on which the electron-hole recombination rate depends. However, the poor separation probability of the photogenerated charge carriers in photocatalytic process severely limits the practical applicability of this green and appealing photocatalytic technology. In addition, some electron-hole pairs will be captured by the defects in the bulk or on the surface of the semiconductor, which deactivate the photocatalytic performance. Therefore, the main obstacle in the field of photocatalysis is to improve the separation efficiency of charge carriers in photocatalysts in the process of environmental cleanup. Up to now, numerous TMOs have been investigated as photocatalysts for application in environmental purification. Many researchers are focused on the development of novel and efficient TMOs. However, the shortcomings of insufficient light absorption and fast recombination of photogenerated charge carriers are obstacles for the practice applications. To this end, a variety of approaches have been proposed to promote the efficiency of photocatalysts, such as heteroatom doping, facet and defect engineering, fabrication of heterojunctions and so on.

Doping with foreign atoms is one of the facilitating and practical approaches to altering the electrical and optical properties and the photocatalytic activity of semiconductors. Usually, some intermediate energy level can be introduced in the forbidden band by doping, which leads to narrowing the bandgap, extending the light-responsive ability,

and enhancing the efficiency of charge carriers' separation. There are many strategies for doping, such as metal doping, non-metal doping, self-doping, co-doping, and so on. Among these methods, anion doping is one of the most promising approaches to enhance photocatalytic performance by the interaction between nonmetal dopants and O 2p electrons in the valence band [14]. The non-metal dopants, such as carbon (C) [15], nitrogen (N) [16], sulfur (S) [17], and fluorine (F) [18], etc., have attracted a great deal of attention. Typically, doping with C and N is widely used since these non-metallic elements have an advantage in narrowing the band gap. In 2001, Asahi et al. reported that the N doping of TiO₂ can increase the visible light photocatalytic activity by sputtering the anatase TiO₂ in an N₂ (40%)/Ar gas mixture followed by annealing in N₂ gas [19]. A significant red shift in the absorption spectra can be achieved by N doping compared to other anionic dopants [20]. Theoretical simulations of the electronic band structures of anatase TiO₂ doped with C, N, F, P, or S substitutional dopants indicated that N doping was the most effective in narrowing the bandgap by overlapping energy states between N 2p and O 2p [19]. Nakamura and coworkers put forward the mechanism for the enhancement of N doping. TiO₂ doped with nitrogen resulted in a mid-gap level (N 2p) above the top of the valence band (O 2p), which reduced the energy gap required for charge separation [21]. During the photoexcitation, the electrons were excited and migrated from the initial valence band into the mid-band gap energy level, leaving holes in the valence band. As a result, the N-doped TiO₂ was introduced with visible-light responsive photocatalytic activity, and the produced impurity level was also beneficial for the separation of charge carriers. Besides the binary metal oxides, N doping is also effective in TMOs to achieve bandgap narrowing, such as N-doped SrSnO₃ and La₂Ti₂O₇ [22,23]. N doping in TMOs resulted in the formation of vacancies that acted as preminent electron capture centers, which could lower the recombination velocity of photo-induced carriers and enhance the photocatalytic degradation performance. However, compared with the N doping in binary metal oxide, the relatively less investigation of N doping and other non-metal doping in TMOs. The detailed experimental investigation of N doping in TMOs should be further conducted towards versatile applications. In addition to N doping, TMOs interaction with N sometimes led to phase transformation to corresponding oxynitrides via ammonolysis reaction under the NH₃ atmosphere. The oxynitrides or some N contained materials with a strong ability to absorb visible light have also been reported effective for the photocatalytic degradation of toxic compounds and offer a wide range of potential applications [24,25]. The narrow bandgap and tunable band position of oxynitride have also attracted much attention in many fields. This review focuses on the recent progress of the effects of N doping of TMOs and oxynitride transformed from TMOs. The possibilities of the enhanced photocatalytic activity of TMOs modified by N anions will be presented. We have discussed selected typical TMOs that are mainly concerned with tunable N doping concentrations, different N doping sites, and phase transformation towards visible-light-induced photocatalytic activity.

2. The Influence of N

TMOs as photocatalysts are greatly influenced by the active sites and the composition, which can dramatically increase the energy conversion or selectivity of catalysts. A common method for changing the active sites is atom doping. Although it is easier to achieve cation doping by the addition of stable metal cationic salts, anions doping is also effective in tuning the lattice and electronic structure of the catalysts, thus inducing various functionality. As one of the widely applied anions, the N can alter the structure and electronic structure of the TMOs, which could further lead to the different physical and chemical properties, such as the bandgap energy, the Fermi level, the localized electronic state, electrical conductivity and so on [26]. Asahi et al. first noted that the valence band maximum of TiO₂ shifted upward by substitutional N doping to form mixing of N 2p and O 2p states, which was indispensable for visible light absorption and high photocatalytic activity [19]. Since then, plenty of works have demonstrated the prominent effect of N doping in narrowing the bandgap of the oxides by different doping methods with various N sources [23,27–29].

N₂ gas mixed with Ar gas was reported as N source to prepare N-doped TiO₂ thin film. Further calcination under N₂ gas led to crystallized TiO₂ with rutile and anatase phases, which was responsive to visible light [19]. In addition, heat treatment under NH₃ gas or with urea is also widely applied to dope N into metal oxides [30–32]. Liu et al. have reported a red TiO₂ by N doping under NH₃ treatment. The pre-doped interstitial boron ions facilitated the substitution of O by N anions, resulting in a high visible light absorption band in B/N codoped TiO₂ [28]. After ball milling of a solid mixture of ZnO and urea with different ratios, a series of the N-doped ZnO was synthesized by calcination under an air atmosphere [33]. Besides the two-steps approach to introduce N, the simple one-pot synthetic method is also an effective strategy for N doping by adding different N sources. The urea can also be used as N source in a wet chemical process. A facile microwave-assisted hydrothermal method was reported to prepare N-doped BiVO₄ with different concentrations of urea in the solution [34]. In the sol-gel reverse micelle method, Na₂EDTA was used as a nitrogen source to prepare N-doped TiO₂ with remarkable photocatalytic activity under visible light irradiation [35]. Therefore, when various methods have been developed to introduce N anion, a better understanding of N doping amounts and doping sites is beneficial to further enhance the photocatalytic activity. This section focuses on the influence of different N doping concentrations, substitutional/interstitial doping sites, and the phase transition to form oxynitride, especially in the TMOs.

2.1. The Influence of N Doping

2.1.1. N Doping Concentration and Doping Site

The N doping led to the formation of a localized state near the valence band of the oxides, which is essential for the tuning of the bandgap energy of TMOs. One of the most important points that should be mentioned is the concentration of N doping. The bandgap usually becomes narrowed as the N doping amount increases. Although the N doping amount was widely studied in the TiO₂ [36], the different doping amounts also affect the optical property, the electronic band structures as well as the photocatalytic activity of complexed N-doped TMOs.

Wang et al. reported that N-doped La₂Ti₂O₇ with various nitrogen doping amounts showed tunable optical absorbance edge and bandgap energy (Figure 1a,b). Compared with the white color of La₂Ti₂O₇ precursor, the N-doped samples exhibited color changed from gray to yellow as the N anions were introduced into the sample (the inset in Figure 1a). An important insight was obtained into the pre-doped N in La₂Ti₂O₇ precursor in weakening the Ti-O bond, allowing the further introduction of N into La₂Ti₂O₇. The DFT calculation also verified that the interaction of the N dopants would reduce the total energy of the systems [37]. The relations between N doping amount with the specific surface area indicated that the more N dopants introduced into La₂Ti₂O₇, the smaller specific surface area could obtain (Figure 1c). This figure also showed that when the N doping amount increased from 3.5 at% to 5.74 at%, the photocatalytic activity increased until an optimal concentration was reached, which should be less than 5%. This series of N-doped La₂Ti₂O₇ samples suggested that there was an optimum N doping amount to obtain the highest visible-light activity. The effect of the nitrogen amounts on the electronic band structures of N-doped La₂Ti₂O₇ was investigated by theoretical calculations [37]. Two different N doping concentrations were investigated, including 1.12–1.14 at% N-doped La₂Ti₂O₇ and 3.30–3.45 at% N-doped La₂Ti₂O₇. Both low and high concentrations of N doping resulted in bandgap narrowing. The isolated N 2p impurity states were formed in the bandgap at lower doping levels. The creation of localized electronic levels above the valence band was primarily responsible for the narrowing of the bandgap of N-doped La₂Ti₂O₇. As the doping concentration increased, the localized N 2p states stretched to lower energies and integrated into the edge of the valence band. In addition to changing the amount of N doping by changing the reaction conditions, such as the reaction time, reaction temperature, and NH₃ flow rate, the different N sources also affect the N doping concentration in TMOs. N-doped SrTiO₃ with various N concentrations was reported with a mechanochemical

approach to incorporate N into the lattice of SrTiO₃ [38]. The same weight percentage of N sources (20 wt% of hexamethylenetetramine, urea, and ammonium carbonate) were mixed with SrTiO₃, respectively. The different N content in these three samples explained that the effect of N precursors on the N doping concentration was different, which also determined the photocatalytic activity.

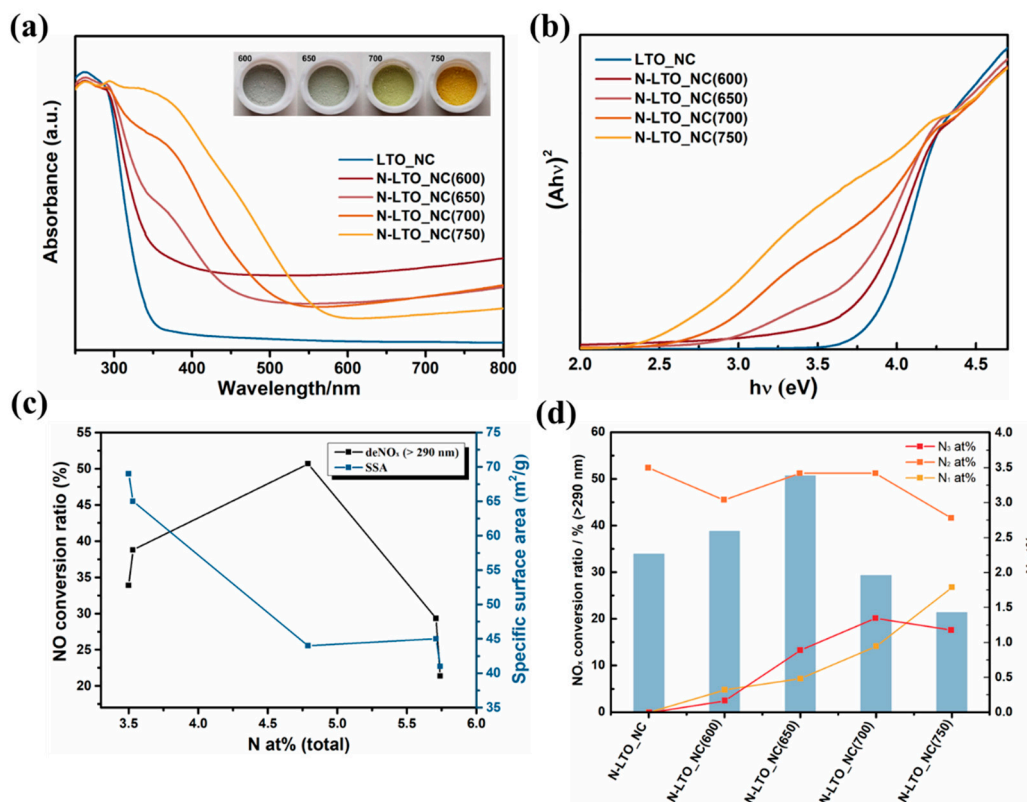


Figure 1. (a) UV-vis diffuse reflectance spectra, (b) Tauc plots of N-doped La₂Ti₂O₇, (c) the relations of total nitrogen amount (at%) with NO conversion ratios and specific surface areas, and (d) correlation between the photocatalytic NO conversion ratio of La₂Ti₂O₇ precursor, N-doped La₂Ti₂O₇ under different calcination temperature (600–750 °C) and different nitrogen sites (N1: substitutional N with N-Ti-N bond, N2: substitutional N with N-Ti-O bond, and N3: interstitial N) [31] (Reproduced from Ref. [31] with permission from the Elsevier).

In addition, the nitrogen doping sites also greatly influence the bandgap energy, electronic structure, and photocatalytic activity of TMOs. In the case of N-doped La₂Ti₂O₇, the substitutional N and interstitial N sites have been thoroughly studied [31]. The pre-doped N in La₂Ti₂O₇ precursor was the substitutional N with N-Ti-O band. After NH₃ treatment, substitutional N with N-Ti-N bond and interstitial N were introduced into N-doped La₂Ti₂O₇ with different contents. As shown in Figure 1d, the photocatalytic deNO_x activity of N-doped La₂Ti₂O₇ was strongly related to the doping sites of the nitrogen. Although, the N-Ti-N bond (N1) and the interstitial N (N3) can possess negative and positive contribution to the visible light photocatalytic activity, respectively. The interstitial N can possess positive contributions to the visible light photocatalytic activity. For substitutional N, there was no obvious correlation between N-Ti-O substitutional N (N2) with photocatalytic activity, while substitutional N with N-Ti-N bond was not beneficial to improve the photocatalytic activity when the high concentration of N doping was applied. Jin et al. have also discussed the effect of intestinal N in Mn_xCo_{3-x}O₄ [39]. The analysis indicated the introduction of interstitial nitrogen changed the coordination of Mn and Co atoms and lattice distortion by the Jahn-Teller effect. The chemical structures of Mn_xCo_{3-x}O₄, interstitial N-Mn_xCo_{3-x}O₄, and substitutional N-Mn_xCo_{3-x}O₄ were shown in Figure 2. The DFT calculation verified

the adsorption energy of aniline on the catalyst surface was negative with N doping, which was beneficial for the adsorption of aniline. Therefore, the high oxidative catalytic performance of the N-Mn_xCo_{3-x}O₄ was achieved. The photocatalytic activity can be greatly influenced by the electronic structure of the semiconductors, which is closely related to the light absorption ability, redox potential, and charge carrier efficiency. The DFT calculations revealed the varied electronic structure of TMOs had a close relation with different N doping sites [37]. The doping N atoms prefer to occupy the interstitial position because of the lower formation energy of interstitial N than that of substitutional N. The calculation results indicated the different N doping sites have different influences on the electronic structure of TMOs. The calculated density of states results indicated that the substitutional N at the O site effectively shifted the valence band edge upward. The introduction of O vacancy by substitutional N also reduced bandgap energy, which will be discussed in the next section.

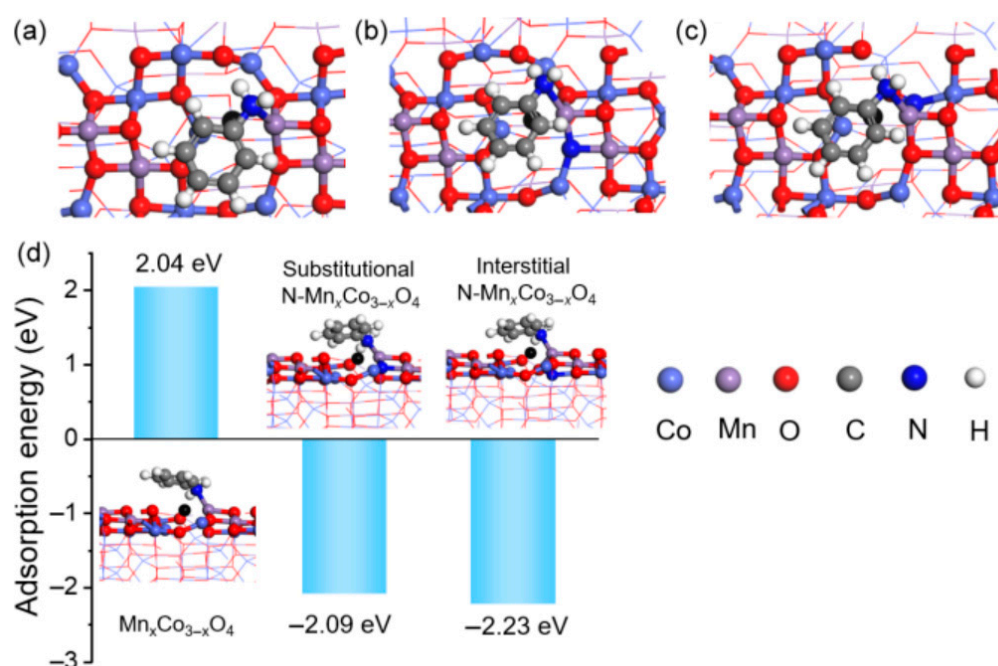


Figure 2. (a–c) the chemical structure of Mn_xCo_{3-x}O₄, interstitial N-Mn_xCo_{3-x}O₄, and substitutional N-Mn_xCo_{3-x}O₄, (d) the DFT calculation of adsorption energy of aniline on the surface of Mn_xCo_{3-x}O₄, interstitial N-Mn_xCo_{3-x}O₄, and substitutional N-Mn_xCo_{3-x}O₄ [39] (Reproduced from Ref. [39] with permission from the Springer).

2.1.2. Defects Induced by N Doping

Defect engineering is an important approach to modulating the physical and chemical properties, such as the surface energy and electronic band structure, therefore efficiently improving the photocatalytic activity of TMOs. Defects in semiconductor photocatalysts have a great impact on the carrier concentration and interface reaction, which can affect the efficiency of the photocatalytic reaction. In general, the reactivity and selectivity of the photocatalysts can be achieved by tuning different kinds of defects. Defects in semiconductors can be classified into four basic divisions based on different dimensions, including zero-dimensional point defects (vacancy and doping), one-dimensional line defects (screw or edge dislocation), two-dimensional planar defects (grain or twin boundary), and three-dimensional volume defects (lattice disorder and void) [40]. However, the defects are deemed to be recombination centers for photogenerated charge carriers and scattering centers for electron and hole traveling, both of which are detrimental to photocatalytic activity. With the development of defect engineering, the positive contribution of defects on photocatalysts with controlled defects can be recognized. The formation of vacancy was reported to enhance the photocatalytic activity and promote the migration of charge

carriers. Kim et al. demonstrated that the introduction of oxygen vacancies into BaSnO₃ could reduce both the recombination of charge carriers and bandgap energy. The precisely controlled bandgap energy should be attributed to the controllable induced oxygen vacancies [41]. The oxygen vacancies, especially on the surface, can be considered as shallow donors, which are beneficial for the adsorption and reaction in the photocatalytic process. The formation of ample oxygen vacancies caused by interstitial N played a significant role in N-Mn_xCo_{3-x}O₄ to promote the surface mobility of oxygen species and enhance aerobic oxidation reaction [39]. The formation of oxygen vacancy may also introduce reduced metal ions due to the charge compensation, for example, Ti³⁺ in N-doped La₂Ti₂O₇. The formed Ti³⁺ could be oxidized to induce O₂^{-•} radicals, which was essential for photocatalytic activity [42]. The electron paramagnetic resonance (EPR) showed that the neutral paramagnetic N_b[•] species in bulk produced from the complexed oxidation in the N doping process played a key role in the photocatalytic activity by reacting with O₂ to produce O₂^{-•} [42,43]. Therefore, it is necessary to investigate the influence of defects in regard to the concentration of charge carriers, transfer dynamics, interface reaction, and band structure [44]. It is important to notice that the growth of crystal facets is always accompanied by the generation of defects. The formation of a specific crystal facet is beneficial for high reactivity due to the favorable surface atomic structures and surface electronic structures [45,46]. The synergistic effects of crystal facet and crystal defect can further facilitate the charge transfer and improve the photocatalytic performance of semiconductors, which could lead to a new horizon in the design of photocatalysts for practical applications.

2.2. Phase Transformation by N Interaction

Although the fact that element doping can induce visible light absorption of the traditional semiconductor photocatalysts, the localized levels generated by impurities may act as recombination sites for charge carriers, which may reduce the photocatalytic activity of the doped materials. In recent years, precise control of the bandgap and electrical/optical properties of semiconductor materials to obtain an optimal balance between optical absorption and redox potentials can be achieved by a phase transformation from TMOs [47–49]. Introduction of N into oxides also leads to the formation of oxynitride or nitride materials [50,51]. Many researchers have focused on the fabrication of oxynitride by topochemical ammonolysis reaction from transition metal oxides to adjust the energy band structure, such as (Ga_{1-x}Zn_x)(N_{1-x}O_x) [52], (Zn_{1+x}Ge)(N₂O_x) [53], ATaO₂N (A = Ca, Sr, Ba) [54], Na_xLa_{1-x}TaO_{1+2x}N_{2-2x} [55] and so on. These oxynitride materials have been demonstrated to exhibit enhanced photocatalytic activity by modulating the band structures.

(Ga_{1-x}Zn_x)(N_{1-x}O_x), a solid solution of GaN and ZnO, has been used as a visible-light responsive photocatalyst for organic pollutants degradation [56] and water splitting [57]. As shown in Figure 3a,b, different absorption edges were observed in (Ga_{1-x}Zn_x)(N_{1-x}O_x) due to the various O/N ratios [58]. The interaction of N with Ga₂O₃ under NH₃ atmosphere resulted in the topochemical transition to form (Ga_{1-x}Zn_x)(N_{1-x}O_x) with visible light absorption ability. The bandgap energy of (Ga_{1-x}Zn_x)(N_{1-x}O_x) showed a decreasing trend with an increasing O/N ratio. The narrowed bandgap should be originated from the p-d repulsion between N 2p/O 2p and Ga 3d states. Besides, the (Ga_{1-x}Zn_x)(N_{1-x}O_x) solid solution with wurtzite structure was also reported to form by phase transformation from spinel ZnGa₂O₄ [59]. A broad range of compositions of (Ga_{1-x}Zn_x)(N_{1-x}O_x) solid solution showed varied absorption edges and bandgap energy (Figure 3c), which were effective for visible-light-driven water oxidation. The varied composition range and band structure could be achieved by different reaction conditions under NH₃ treatment. Therefore, the obtained sample showed interesting physical and chemical properties for photocatalytic activity. The interaction with N via ammonolysis reaction also resulted in the phase transformation of other TMOs, such as Zn₂GeO₄ to (Zn_{1+x}Ge)(N₂O_x) [60], La₂Ti₂O₇ to LaTiO₂N [61], Ba₂Ta₂O₇ to BaTaO₂N [62], etc.

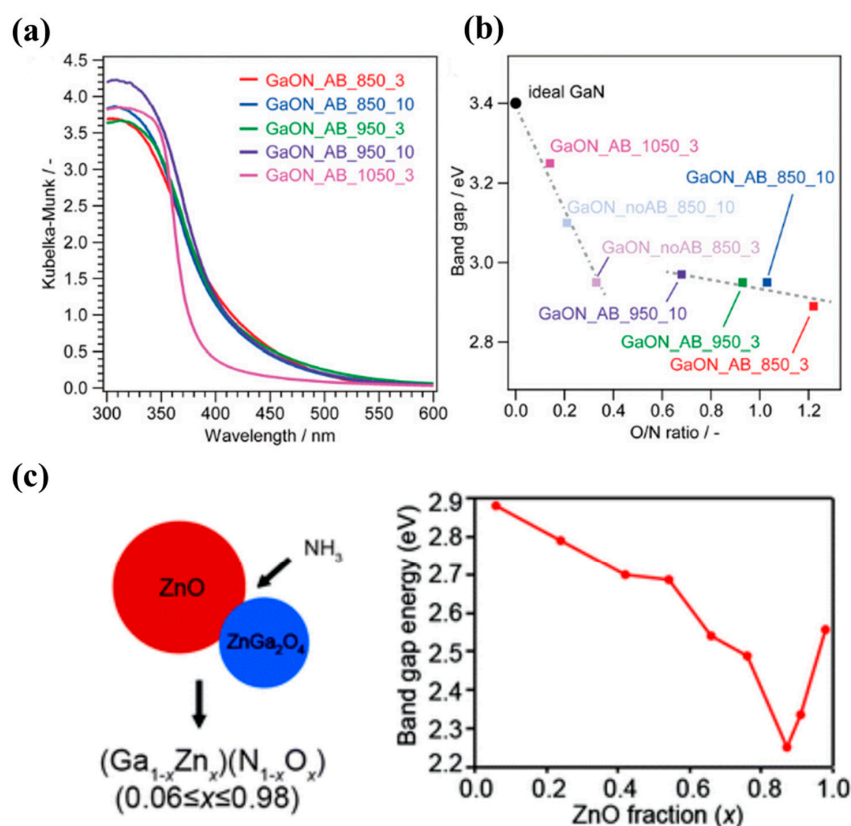


Figure 3. (a) UV-vis DRS spectra of the $(\text{Ga}_{1-x}\text{Zn}_x)(\text{N}_{1-x}\text{O}_x)$ samples. (b) Relationship between the O/N ratio and the band gap of $(\text{Ga}_{1-x}\text{Zn}_x)(\text{N}_{1-x}\text{O}_x)$, [58] and (c) the relations between bandgap energies and ZnO fraction (x) in $(\text{Ga}_{1-x}\text{Zn}_x)(\text{N}_{1-x}\text{O}_x)$ solid solutions [59] (Reproduced from Refs. [58,59] with permission from the RSC).

3. Recent Advances in Nitrogen Modified in TMOs

Metal oxides have been widely studied as semiconductor photocatalysts, especially the binary oxides, since TiO_2 was applied as a photocatalyst for water splitting in the 1970s [1]. Compared with the simple binary metal oxides, the TMOs possess a more complex composition, chemical bonding between different cations and oxygen atoms, and flexible crystal structure. Therefore, TMOs sometimes exhibit interesting properties and functionalities, which are less pronounced or even absent in binary metal oxides [63]. The complex structure offers significant advantages for TMOs as photocatalysts. First, the band edge potentials for TMOs are suitable for various photoinduced reactions. In addition, the presence of different metal ions in the lattice of TMOs allows for more flexibility in designing and modifying the band structure as well as other photophysical properties. By band structure engineering, the ability of solar harvesting and photon-exciton energy conversion can be optimized, such as the fabrication of heterojunctions and the creation of defect states [64]. Therefore, it is necessary and promising to establish a material design principle for TMOs with high photocatalytic activity and stability. The N as an effective hetero-atom can be applied to tune the physiochemical properties and electronic structure of TMOs, consequently improving their catalytic performance. In this section, we summarized the typical TMOs with modification by N anion, including $\text{La}_2\text{Ti}_2\text{O}_7$ and Zn_2GeO_4 . The influence of N doping and the formation of oxynitride is summarized. The summarization of specific TMOs can provide useful information for further analyzing other TMOs.

3.1. N-Doped $\text{La}_2\text{Ti}_2\text{O}_7$ and LaTiO_2N

$\text{La}_2\text{Ti}_2\text{O}_7$ (LTO) is a perovskite-type photocatalyst with a layered structure, which is extensively applied in photocatalytic water splitting, CO_2 reduction, and degradation of harmful pollutants [65,66]. The crystal structure of $\text{La}_2\text{Ti}_2\text{O}_7$ is periodically arranged by

corner-sharing TiO_6 octahedra and coordinated lanthanum cations. The network of octahedrons in the $\text{La}_2\text{Ti}_2\text{O}_7$ structure boosts charge carrier mobility, resulting in high quantum yields, especially in photocatalytic reactions. $\text{La}_2\text{Ti}_2\text{O}_7$ possesses a layered structure, and the thickness varies from different preparation methods. Hydrothermal reactions are widely used to fabricate $\text{La}_2\text{Ti}_2\text{O}_7$ with small particle size [67,68]. The molten salt flux method can also be applied to synthesize $\text{La}_2\text{Ti}_2\text{O}_7$ with different morphologies and big particle sizes by using the Na_2MoO_4 , K_2MoO_4 , NaCl , and mixed $\text{NaCl} + \text{K}_2\text{MoO}_4$ fluxes [69]. The different synthetic conditions of nucleation, the growth rate in each crystalline direction, and thermodynamic or kinetic balance influence the crystal shape and thickness of the obtained $\text{La}_2\text{Ti}_2\text{O}_7$ crystals. Among these synthetic methods, the hydrothermal reaction is widely applied to develop $\text{La}_2\text{Ti}_2\text{O}_7$ nanostructure with a high specific surface area, which boosts the separation and mobility of charge carriers to increase photocatalytic activity [70].

Unfortunately, the large bandgap of $\text{La}_2\text{Ti}_2\text{O}_7$ (3.0–4.0 eV) renders this semiconductor only active under UV light irradiation. Therefore, many efforts have been made to improve the visible light absorption and efficiency of photoexcited charge separation. Doping heteroatoms is identified as an effective and promising method to enlarge the range of light absorption and enhance the performance of the catalysts. The electric structure of $\text{La}_2\text{Ti}_2\text{O}_7$ can be easily altered by substituting La and Ti atoms with other heteroatoms due to its layered structure formed by the TiO_6 octahedra units and La atoms in the interlayer, such as V, Cr, or Fe-doped $\text{La}_2\text{Ti}_2\text{O}_7$ [65,71]. Although cation doping into $\text{La}_2\text{Ti}_2\text{O}_7$ has been reported, the nitrogen anion is widely applied and identified as an effective dopant in the experiment and thermotical analysis. Meng et al. have synthesized $\text{La}_2\text{Ti}_2\text{O}_7$ with a hydrothermal method and treated the precursor with NH_3 flow. The obtained N-doped $\text{La}_2\text{Ti}_2\text{O}_7$ showed a nanosheet morphology with a bandgap of 2.51 eV, which was much narrower than that of the $\text{La}_2\text{Ti}_2\text{O}_7$ precursor [72]. The author stated that the introduced N anion led to the formation of a continuous upward shift of the valence band edge, which was observed from the parallel shift of the absorption edge. The narrowed bandgap of N-doped $\text{La}_2\text{Ti}_2\text{O}_7$ originated from the hybridization of N 2p and O 2p states. Compared with the pristine $\text{La}_2\text{Ti}_2\text{O}_7$, the N dopants in $\text{La}_2\text{Ti}_2\text{O}_7$ enhanced the light absorption, and the delocalized photogenerated electrons and holes facilitated the photocatalytic decomposition of methyl orange under UV and visible light irradiation. The research by Wang et al. has indicated that the parallel shift of the absorption edge did not always boost the photocatalytic activity [31]. The light absorption varied from the concentration of introduced N atoms. Although a parallel shift of absorption edge was achieved by NH_3 treatment at 750 °C, this sample with the highest N doping amount showed declined photocatalytic deNO_x activity. In this research, N doping in $\text{La}_2\text{Ti}_2\text{O}_7$ at lower temperatures resulted in an add-on shoulder in the cutoff edge of the absorption spectrum, indicating the generation of localized states between the bandgap of $\text{La}_2\text{Ti}_2\text{O}_7$ by N dopants [73]. The localized N 2p state probably originated from the pre-doped N in $\text{La}_2\text{Ti}_2\text{O}_7$ precursor from the hydrothermal reaction. The author applied triethanolamine as an additive, which acted as an agent to control the morphology and N source for pre-doping. The high concentration of N doping after the nitridation with NH_3 may be caused by the pre-doped N. The pre-doped N in the $\text{La}_2\text{Ti}_2\text{O}_7$ precursor was characterized as substitutional N with N-Ti-O bond, which was essential for the further N doping process by NH_3 treatment. N-doped $\text{La}_2\text{Ti}_2\text{O}_7$ calcinated at 650 °C showed the best photocatalytic activity. This result indicated that the N doping amount played an important role in the photocatalytic reaction. The modest dopant-induced states within the bandgap could offer more photogenerated electrons and additional pathways for charge transfer, which was beneficial for the enhancement of photocatalytic activity [74].

Due to the two-dimensional (2D) layered structure and remarkable chemical stability of $\text{La}_2\text{Ti}_2\text{O}_7$, many researchers fabricated the heterojunctions to improve the light-harvesting, separation efficiency of photogenerated charge carriers, and transfer rate of electrons, such as $\text{Ag}_2\text{PO}_4/\text{La}_2\text{Ti}_2\text{O}_7$, $\text{BiOBr}/\text{La}_2\text{Ti}_2\text{O}_7$, and $\text{g-C}_3\text{N}_4/\text{La}_2\text{Ti}_2\text{O}_7$ [75–77]. Coupling with a semiconductor with a suitable band position and a narrow bandgap is important in

fabricating heterojunctions with $\text{La}_2\text{Ti}_2\text{O}_7$. Besides simply combining with $\text{La}_2\text{Ti}_2\text{O}_7$, band gap engineering by N dopant for $\text{La}_2\text{Ti}_2\text{O}_7$ to induce visible light absorption ability is also a good choice for the fabrication of composite, which was summarized in Table 1. Reduced graphene oxide (rGO) with its unique one-atom layered structure and fascinating chemical properties has attracted great attention and boosted research toward diverse catalytic reactions, such as photocatalytic selective oxidation of cyclohexane, photocatalytic O_2 evolution, lithium-ion batteries, and so on [78–80]. Besides, rGO with high electronic conductivity has significant implications for anchoring other semiconductors to fabricate composite, which can facilitate electron transfer. N-doped $\text{La}_2\text{Ti}_2\text{O}_7$ has been reported to be assembled with rGO by Hua et al. [81]. Compared with the bare $\text{La}_2\text{Ti}_2\text{O}_7$, the introduction of N could enhance the electron transfer, while the lifetime of charge carriers greatly prolonged in N-LTO/rGO composite due to the synergistic effect of N doping and rGO assembling. Besides, Au and Pt nanoparticles have also been reported as an electron relay to increase the charge separation in the ternary composite, Au@Pt-N-LTO/rGO [82]. The deposition of metal nanoparticles, especially Au, played an essential role in extending visible light absorption. Compared solely hybridized with rGO, the ternary composite with metal nanoparticles extended the light absorption up to 600 nm and further enhanced the charge carrier lifetime. On the other hand, a change in the flat band potential occurred by the deposition of Au nanoparticles on the surface of N-LTO, which altered the band alignment and improved the charge extraction to achieve high photocatalytic H_2 generation activity. $\text{g-C}_3\text{N}_4$ is a metal-free semiconductor with a stacking 2D layered structure and visible-light response, which has attracted attention in the environmental remediation field [83]. The low solar radiation absorption and poor charge separation leave a lot of space for improvement of bare $\text{g-C}_3\text{N}_4$. Cai and coworkers successfully prepared a composite of $\text{g-C}_3\text{N}_4$ and N-doped $\text{La}_2\text{Ti}_2\text{O}_7$ nanosheets with a hybridized 2D layered structure to promote the spatial separation and interchange of charge carriers [73]. The large interface area and short interfacial distance could be achieved by this 2D/2D heterostructure, which resulted in the decreased recombination of charge carriers. The fast transport of photogenerated electrons was attributed to the formation of a built-in field induced by the difference in chemical potential between N-doped $\text{La}_2\text{Ti}_2\text{O}_7$ and $\text{g-C}_3\text{N}_4$. In addition, the 2D/2D heterojunction was also achieved by Xia et al. by the combination of N-doped $\text{La}_2\text{Ti}_2\text{O}_7$ and ZnIn_2S_4 . The conduction band potential of ZnIn_2S_4 is suitable for the fabrication with $\text{La}_2\text{Ti}_2\text{O}_7$ to induce a large surface area, which could provide many reaction sites and facilitate the mass transfer. The composite could be synthesized by the hydrothermal reaction by directly growing ZnIn_2S_4 on the surface of N-doped $\text{La}_2\text{Ti}_2\text{O}_7$. The formation of an intimate interfacial contact interface can generate short charge transfer channels and accelerate the migration of electrons or holes. N-LTO/ ZnIn_2S_4 with appropriate positions of the valence and conduction bands and enhanced light absorption capacity by N doping exhibited high photocatalytic hydrogen evolution activity. The above studies showed that researchers could fabricate heterojunction structures with matched energy bands and large interfacial contacts to further boost the high efficiency of visible-light photocatalytic activity.

Table 1. Summary of the N-doped $\text{La}_2\text{Ti}_2\text{O}_7$ (N-LTO) and its composites for photocatalytic based reactions.

| Photocatalyst | N Doping Method | Bandgap Energy (eV) | N Amount (at. %) | Target Photocatalytic Reaction | Ref |
|----------------------------------|--------------------------------------|---------------------|------------------|--|------|
| N-LTO | NH_3 treatment | 2.51 | 3.3 | Decomposition of methyl orange under UV and visible light | [23] |
| N-LTO | NH_3 treatment | 2.84 | 4.79 | Decomposition of NO_x under UV and visible light | [31] |
| N-LTO/rGO | NH_3 treatment | 2.88 | 2.1 | Decomposition of bisphenol A under UV and visible light | [81] |
| N-LTO/ $\text{g-C}_3\text{N}_4$ | Hydrothermal method + acid treatment | 2.65 | 5.8 | Degradation of MO and reductive generation of H_2 under visible light | [73] |
| N-LTO/ ZnIn_2S_4 | Hydrothermal method + acid treatment | 3.35 | - | H_2 evolution reaction | [84] |
| Au@Pt-N-LTO/rGO | NH_3 treatment | 2.25 | - | H_2 evolution reaction | [82] |

During the NH_3 treatment at high temperatures or for a long reaction time, more O ions in LaTi_2O_7 can be substituted by N ions. $\text{La}_2\text{Ti}_2\text{O}_7$ precursor further interacted with N, resulting in the phase transformation from $\text{La}_2\text{Ti}_2\text{O}_7$ to LaTiO_2N . LaTiO_2N is one of the well-known perovskite oxynitrides with the capability to absorb the long wavelength of light up to ca. 600 nm. Compared with N doping, the modified $\text{La}_2\text{Ti}_2\text{O}_7$ by phase transformation to oxynitride can further boost the visible light absorption ability. Moreover, LaTiO_2N can form a solid solution with other perovskite oxides and oxynitrides [85]. It is an n-type semiconductor and processes thermal and chemical stability making it suitable to be applied as a visible-light-driven photocatalyst [85]. Another advantage of LaTiO_2N is that the component elements are relatively abundant, inexpensive, and non-toxic [85]. Many researchers focused on this material with unique photocatalytic, optical, and dielectric properties to be applied mainly in water splitting for H_2 or O_2 production in the presence of sacrificial reagents [86–88]. Matsukawa et al. have reported surface reconstruction of LaTiO_2N particles by nitriding $\text{La}_2\text{Ti}_2\text{O}_7$ precursor at 1223 K for 15 h under an NH_3 flow [89]. The high reaction temperature and long reaction time led to phase transformation by nitridation from the surface toward the bulk of the particles. LaTiO_2N was further treated by aqua regia to eliminate the surface defects, which can double the photocatalytic performance in H_2 and O_2 evolution under irradiation of visible light. Li and colleagues prepared LaTiO_2N with a hollow sphere structure, which enabled fast charge carrier migration because of the short diffusion distance [90]. The H_2 -treated LaTiO_2N exhibited a distorted surface layer, which could suppress the recombination of photo-generated carriers and enhance the quantum efficiency for H_2 generation under visible light irradiation. Therefore, the phase transformation from $\text{La}_2\text{Ti}_2\text{O}_7$ to LaTiO_2N can boost the absorption of visible light, and the photocatalytic activity of LaTiO_2N can be improved by further treatment.

3.2. N-Doped Zn_2GeO_4 and $(\text{Zn}_{1+x}\text{Ge})(\text{N}_2\text{O}_x)$

Zinc germanate (Zn_2GeO_4) is a chemically and thermally stable ternary metal oxide with a rhombohedral structure. Recently, compared with the photocatalysts composed of d^0 elements (e.g., TiO_2), Zn_2GeO_4 with d^{10} configuration (Zn^{2+} and Ge^{4+}) has attracted significant attention because of its high chemical and thermal stability, optical properties, and broad functionality. The development of photocatalysts has shifted to semiconductors composed of d^{10} elements because the largely dispersed hybridized s-p orbitals in conduction bands have the capacity to produce highly mobile photoexcited electrons [91]. Figure 4a,b exhibit the crystal structure of Zn_2GeO_4 . It possesses a rhombohedral structure with an R3 space group and comprises GeO_4 and ZnO_4 tetrahedra. In a hexagonal unit cell, two different types of ZnO_4 tetrahedra and one GeO_4 tetrahedron are coupled with one another and connected by oxygen atoms. Zn ions are in two different crystallographic positions with different bond distances [92]. Zn_2GeO_4 has been widely used in anode materials for lithium batteries, photocatalysis to remove heavy metal or organic pollutants, electrochemical sensors, and phosphors for lighting and display devices [93–96]. For example, amorphous Zn_2GeO_4 nanoparticles demonstrated a high reversible specific capacity and outstanding rate capability when used as anode materials for Li-ion batteries [97]. RuO_2 -dispersed Zn_2GeO_4 was discovered to be applied as a photocatalyst with excellent activity for water splitting to generate H_2 and O_2 [98]. Zn_2GeO_4 with nanorods and large flower-shaped particle morphologies possesses effective photocatalytic activity for dye degradation [99]. Zn_2GeO_4 nanorods with exposed (110) facets also showed high performance in the photocatalytic conversion of CO_2 and H_2O to hydrocarbon fuels [100].

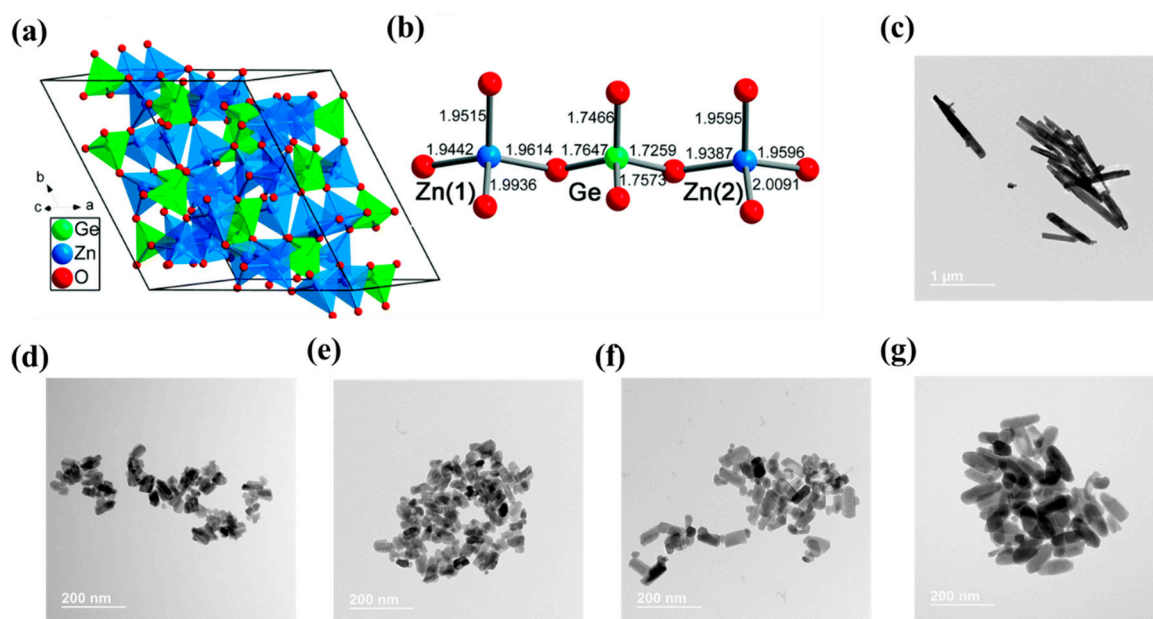


Figure 4. (a) Crystal structure of Zn_2GeO_4 (blue tetrahedra: ZnO_4 ; green octahedra: GeO_6), (b) coordination environment of the Zn^{2+} and Ge^{4+} ions in this structure [92], TEM images of Zn_2GeO_4 samples synthesized with different TEA volumes: (c) 0 mL, (d) 2 mL, (e) 4 mL, (f) 6 mL and (g) 8 mL [60] (Reproduced from Refs. [60,92] with permission from the RSC).

Although Zn_2GeO_4 with d^{10} configuration is a promising photocatalyst, the large intrinsic band gap of Zn_2GeO_4 (4.5 eV) [93] only responds to UV light and restricts the absorption of visible light. Therefore, the enhancement of visible light absorption and charge carriers' separation is essential for the better photocatalytic performance of Zn_2GeO_4 . Recent researches have been focusing on extending the light absorption ability of Zn_2GeO_4 by anion doping to modulate its electronic structure. N doping is also one of the effective strategies to enhance visible light absorption. Lu et al. have reported the synthesis of N-doped Zn_2GeO_4 with high crystallinity and purity by a one-pot solvothermal method [101]. The varied amount of urea added in solvothermal resulted in the different concentrations of N doping. There are several oxygen vacancies on the surface of the N- Zn_2GeO_4 catalysts, as evidenced by the atomic ratios of Zn to Ge (1.9:1) and O to Ge (3.3:1). The N doping decreased the bandgap of Zn_2GeO_4 , while the absorption edge was still in UV region. Lan et al. also reported the effect of N doping on the optical property and structural morphology of Zn_2GeO_4 [102]. The N-doped Zn_2GeO_4 applied as a phosphor showed a blue shift in the band region emission due to the oxygen vacancy, Zn interstitial, and Zn/Ge vacancy by N doping. However, the N doping is not very effective in narrowing the bandgap energy of Zn_2GeO_4 , probably because of the limited solubility of the dopant and the formation of some compensating defects. Some references also confirm that the low concentration of N dopant results in the isolated N 2p slightly above the top of the valence band with slight band gap adjustment [103,104]. Since the charged defects and electronic structure of semiconductors can be reduced by co-doping donor-acceptor pairs, introducing another dopant with N dopant effectively enhances the performance of a photocatalyst. A theoretical study by Li et al. has revealed the impact of N and F co-doping on the geometric and electronic structures of Zn_2GeO_4 [105]. The DFT calculation indicated that mono-doping of N or F showed a slightly narrow bandgap than that of the pure Zn_2GeO_4 , especially for the F doping. The N and F co-doping resulted in the mixed valence band structure composed of N 2p, F 2p, and O 2p states, significantly reducing the bandgap energy of Zn_2GeO_4 .

Recently, mixed-anion compounds with more than one anionic species in a single phase possess unique chemical/physical properties and functionalities [48]. Because it is not very effective to modify Zn_2GeO_4 by N doping, the optical and electronic structure

can be altered by elements implantation to form oxynitride with mixed anions of N and O. Zinc germanium oxynitride ($(\text{Zn}_{1+x}\text{Ge})(\text{N}_2\text{O}_x)$), a solid-state solution between ZnO and ZnGeN_2 , is a promising visible-light-induced photocatalyst due to its chemical and thermal stability and shallow band gap less than 3 eV. The $(\text{Zn}_{1+x}\text{Ge})(\text{N}_2\text{O}_x)$ could be synthesized by calcination of ZnO and GeO_2 under NH_3 flow at high temperatures [53,106]. However, some residuals have remained, and the morphology and particle size of the obtained sample was difficult to control. The Zn_2GeO_4 was applied as the precursor to fabricate $(\text{Zn}_{1+x}\text{Ge})(\text{N}_2\text{O}_x)$. The N anions were introduced in Zn_2GeO_4 and substituted O to form the $(\text{Zn}_{1+x}\text{Ge})(\text{N}_2\text{O}_x)$ with wurtzite structure. It should be noted that not only the inherent physical properties but also the morphology, particle size, exposed facet, and surface arrangement of the crystals affect the photocatalytic activity.

$(\text{Zn}_{1+x}\text{Ge})(\text{N}_2\text{O}_x)$ can maintain the morphology and particle size of Zn_2GeO_4 after nitridation or form a hollow structure [60,107]. Therefore, controlling the morphology of the Zn_2GeO_4 precursor is an effective strategy. So far, numerous approaches have been developed to synthesize Zn_2GeO_4 , including conventional solid-state reaction [108], facile microwave-assisted solution-phase approach [109], hydrothermal or solvothermal reaction [100,110,111], ion-exchange route [97,112], low-temperature solution phase route [98]. The solid-state reaction method with the requirement of high reaction temperature usually possesses the drawback of abundant defects, big particle size, and low surface area, which is not beneficial for photocatalytic activity. With regard to the wet chemistry synthetic methods, the more homogenous and nanosized Zn_2GeO_4 can be obtained by easily adjusting the solvent component, surfactant, reaction time, and precursor concentration. For example, the hyperbranched Zn_2GeO_4 nano-architectures in a binary ethylenediamine/water solvent system were synthesized by varying the reaction time from 2 to 24 h via a crystal-splitting growth mechanism [113]. By varying the acid radical in the zinc salt precursor, the morphology and aspect ratio of Zn_2GeO_4 nanorods can be controlled [100].

Nanostructured Zn_2GeO_4 can accelerate the migration of photoexcited charge carriers to reaction sites on the outer surfaces through short pathway [114]. The Zn_2GeO_4 nanoparticle with an average length of 50 nm synthesized by hydrothermal reaction under the presence of TEA (triethanolamine) as an additive was reported by Wang and coauthors [60]. After treatment under NH_3 flow, the obtained oxynitrides reflected the morphology and size of the oxide precursors. This research highlighted the influence of initial metal concentration and the amount of TEA additive in controlling the morphology of the Zn_2GeO_4 . The smaller particle sizes were produced during the hydrothermal reaction as the metal concentration in the starting solution increased. However, substantial agglomeration was produced at higher metal concentrations as a result of the production of many nuclei. As the TEA volume increased, the morphology of the obtained Zn_2GeO_4 changed from nanorods to nanoparticles with a homogenous size because the TEA molecules absorbed on the surface of the nuclei inhibited the growth (Figure 4c–g). After the introduction of N into Zn_2GeO_4 to substitute O, $(\text{Zn}_{1+x}\text{Ge})(\text{N}_2\text{O}_x)$ exhibited an extended light absorption to around 468 nm. After nitridation, the large intrinsic band gap of Zn_2GeO_4 can be greatly reduced, inducing visible light absorption. Because of the reductive atmosphere, the holes appeared on the surface or inside the particle due to the evaporation of zinc. The high surface area of $(\text{Zn}_{1+x}\text{Ge})(\text{N}_2\text{O}_x)$ can provide more active sites for the photocatalytic reaction. Besides, the nitridation process introduced different concentrations of N with various reaction times. The atomic ratio of O/N exhibited a decreasing trend with the increase in nitridation time, indicating that more O was substituted by N in the crystal structure. As mentioned above, the morphology of the Zn_2GeO_4 precursor influenced the shape and size of the $(\text{Zn}_{1+x}\text{Ge})(\text{N}_2\text{O}_x)$. A unique hollow structure of $(\text{Zn}_{1+x}\text{Ge})(\text{N}_2\text{O}_x)$ was also reported by nitridation under NH_3 flow. The introduction of N into Zn_2GeO_4 nanorod led to the phase transformation to $(\text{Zn}_{1+x}\text{Ge})(\text{N}_2\text{O}_x)$ with nanotube morphology. The $(\text{Zn}_{1+x}\text{Ge})(\text{N}_2\text{O}_x)$ also showed a red shift absorption edge up to 490 nm with visible light responsivity. The upward shift of the valence band maximum and narrow bandgap of $(\text{Zn}_{1+x}\text{Ge})(\text{N}_2\text{O}_x)$ were attributed to the p-d repulsion between Zn 3d and N 2p/O 2p

orbitals. Besides the visible light absorption ability, the phase transformation by N implantation into Zn_2GeO_4 led to the crystal structure change. In other words, the hollow structure was ascribed to the ordered crystal structure conversion from the [001] direction of rhombohedral nanorod into the [0–10] direction of wurtzite nanotube. Therefore, the phase transformation from Zn_2GeO_4 to $(\text{Zn}_{1+x}\text{Ge})(\text{N}_2\text{O}_x)$ and nanocrystallization to form a hollow structure can result in the enhancement of visible light absorption and the promotion of charge carriers' separation and migration. The obtained $(\text{Zn}_{1+x}\text{Ge})(\text{N}_2\text{O}_x)$ sample showed high photocatalytic decomposition activity of NO_x under visible light irradiation. The above results indicated that the N implantation is a valid strategy to modify Zn_2GeO_4 by phase transformation. Nitridation to form $(\text{Zn}_{1+x}\text{Ge})(\text{N}_2\text{O}_x)$ is more effective than N doping to reduce the bandgap energy and induce high photocatalytic activity.

4. Summary and Perspectives

This review mainly focuses on the development of TMOs materials in the field of photocatalysis with the modification of N anions, including N doping and the formation of oxynitride. Since the DFT calculation first demonstrated the effect of N dopant in TiO_2 , various studies on N-doped photocatalysts have been reported for the purpose of activating photocatalytic reactions in the visible-light region. The effective N dopant possessed the potential to alter the composition, crystal structure, and chemical bonding of TMOs, leading to some interesting properties and functionality. The bandgap energy and electronic structure of TMOs can be tuned by the introduction of N anions, which can enhance photocatalytic activities under visible light irradiation. Besides the bandgap, the photocatalytic activities of TMOs are also affected by plenty of factors, such as particle size, morphology, crystallinity, crystal facets, defects, and so on. The introduction of N into TMOs can influence these factors to achieve better photocatalytic performance. Firstly, we have provided a concise summary of the preparation method for the introduction of N anion with different N sources. Different synthetic methods affect not only the morphology of obtained TMOs, but also the concentration of N doping. TMOs with a large surface are much easier to dope with additional N atoms. However, the high concentration of N doping does not signify high photocatalytic activity because the impurity states might lead to more recombination of charge carriers. It is ideal for achieving an optimal N doping amount in TMOs to induce higher photocatalytic activity than the precursor. N doping sites also greatly influence the bandgap energy, electronic structure, and photocatalytic activity of TMOs. The substitutional N with different bonds or interstitial N can change the coordination of metal cations in TMOs. The different doping sites show diverse contributions to photocatalytic activity. Defects are created concomitantly with heteroatom doping and have the ability to alter physical and chemical properties such as surface energy and electronic band structure. Defect engineering by N doping to introduce appropriate amounts of vacancies is effective in improving the photocatalytic activity of TMOs. Besides, the interaction with N can also result in the phase transformation from TMOs to the corresponding oxynitride. The oxynitride materials usually possess a longer absorption range in visible light than N doping in TMOs. The bandgap energy, electronic structure, and photocatalytic activity can be altered by tuning the composition of oxynitride, especially the ratio of N and O anion. In this review, the typical TMOs, including $\text{La}_2\text{Ti}_2\text{O}_7$ and Zn_2GeO_4 , were summarized for the investigation of N anion on the photocatalytic activity. They both possess wide bandgap energy, which is responsive only to UV light. The N doping and phase transformation to oxynitrides can reduce the bandgap and improve the utilization of solar energy. The tunable N doping amount and sites could be controlled by varying the temperature of the NH_3 treatment. The separation and migration of charge carriers could also be facilitated by N dopants. Although the formation of oxynitride greatly reduced the bandgap energy, the oxidation ability of oxynitride was also reduced. Therefore, oxynitride materials are more effective in O_2/H_2 evolution than the degradation of contaminants. It is crucial to conduct more research on various TMOs to determine the precise mechanism of bandgap reduction and the impact of N doping sites in the bulk and surface of N-doped

TMOs. The research on the N insertion has provided some valuable guidelines for the future development of N-doped TMOs and oxynitride catalysts for photocatalytic reactions. The effectiveness of N-doped TMOs under various light sources, ranging from natural sunlight to artificial visible light irradiation, should be examined from a practical aspect. The non-toxic and feasible synthesized N-doped TMOs with high chemical stability are the future trend for photocatalysis-based reactions. Besides, these materials possess a wide range of potential applications, such as textile fibers with antibacterial and deodorizing functionality, interior materials for indoor to eliminate the odors and VOCs, visible-light-sensitive air purification systems, and so on. This review addresses the modification of TMOs via N doping or phase transformation to oxynitride towards high activity, selective, and stable photocatalysts. It is expected that more N-doped TMOs with unique properties, excellent selectivity, and high stability will be synthesized and applied in the field of energy and environment problems.

Author Contributions: Conceptualization, J.W.; methodology, J.W.; validation, J.W., Y.A., T.H. and S.Y.; investigation, J.W., Y.A., T.H. and S.Y.; resources, J.W.; data curation, J.W.; writing—original draft preparation, J.W.; writing—review and editing, J.W., Y.A., T.H. and S.Y.; visualization, J.W.; supervision, S.Y.; project administration, J.W.; funding acquisition, S.Y. All authors have read and agreed to the published version of the manuscript.

Funding: This work was supported by the Japan Society funded the present work for the Promotion of Science (JSPS) Grant-in-Aid for the Scientific Research (KAKENHI, No. 16H06439; 20H00297), and by the Dynamic Alliance for Open Innovations Bridging Human, Environment and Materials, the Cooperative Research Program of “Network Joint Research Centre for Materials and Devices”.

Conflicts of Interest: The authors declare that they have no competing financial interests or personal relationships that could have appeared to influence the work reported in this paper.

References

1. Fujishima, A.; Honda, K. Electrochemical photolysis of water at a semiconductor electrode. *Nature* **1972**, *238*, 37–38. [[CrossRef](#)] [[PubMed](#)]
2. Yin, S. Creation of advanced optical responsive functionality of ceramics by green processes. *J. Ceram. Soc. Jpn.* **2015**, *123*, 823–834. [[CrossRef](#)]
3. Yin, S.; Asakura, Y. Recent research progress on mixed valence state tungsten based materials. *Tungsten* **2019**, *1*, 5–18. [[CrossRef](#)]
4. Yin, S.; Hasegawa, T. Morphology Control of Transition Metal Oxides by Liquid-Phase Process and Their Material Development. *KONA Powder Part. J.* **2022**, 2023015. [[CrossRef](#)]
5. Xue, Y.; Yin, S. Element doping: A marvelous strategy for pioneering the smart applications of VO₂. *Nanoscale* **2022**, *14*, 11054–11097. [[CrossRef](#)] [[PubMed](#)]
6. Zhao, Z.; Fan, J.; Chang, H.; Asakura, Y.; Yin, S. Recent progress on mixed-anion type visible-light induced photocatalysts. *Sci. China Technol. Sci.* **2017**, *60*, 1447–1457. [[CrossRef](#)]
7. Li, H.; Yin, S.; Wang, Y.; Sato, T. Current progress on persistent fluorescence-assisted composite photocatalysts. *Funct. Mater. Lett.* **2013**, *6*, 1330005. [[CrossRef](#)]
8. Linsebigler, A.L.; Lu, G.; Yates Jr, J.T. Photocatalysis on TiO₂ surfaces: Principles, mechanisms, and selected results. *Chem. Rev.* **1995**, *95*, 735–758. [[CrossRef](#)]
9. Wang, R.; Hashimoto, K.; Fujishima, A.; Chikuni, M.; Kojima, E.; Kitamura, A.; Shimohigoshi, M.; Watanabe, T. Light-induced amphiphilic surfaces. *Nature* **1997**, *388*, 431–432. [[CrossRef](#)]
10. Wu, X.; Yin, S.; Dong, Q.; Liu, B.; Wang, Y.; Sekino, T.; Lee, S.W.; Sato, T. UV, visible and near-infrared lights induced NO_x destruction activity of (Yb, Er)-NaYF₄/C-TiO₂ composite. *Sci. Rep.* **2013**, *3*, 2918. [[CrossRef](#)]
11. Komatsuda, S.; Asakura, Y.; Vequizo, J.J.M.; Yamakata, A.; Yin, S. Enhanced photocatalytic NO_x decomposition of visible-light responsive F-TiO₂/(N, C)-TiO₂ by charge transfer between F-TiO₂ and (N, C)-TiO₂ through their doping levels. *Appl. Catal. B* **2018**, *238*, 358–364. [[CrossRef](#)]
12. Noda, C.; Asakura, Y.; Shiraki, K.; Yamakata, A.; Yin, S. Synthesis of three-component C₃N₄/rGO/C-TiO₂ photocatalyst with enhanced visible-light responsive photocatalytic deNO_x activity. *Chem. Eng. J.* **2020**, *390*, 124616. [[CrossRef](#)]
13. Gu, Z.; Cui, Z.; Wang, Z.; Qin, K.S.; Asakura, Y.; Hasegawa, T.; Tsukuda, S.; Hongo, K.; Maezono, R.; Yin, S. Carbon vacancies and hydroxyls in graphitic carbon nitride: Promoted photocatalytic NO removal activity and mechanism. *Appl. Catal. B* **2020**, *279*, 119376. [[CrossRef](#)]
14. Fujishima, A.; Zhang, X.; Tryk, D.A. TiO₂ photocatalysis and related surface phenomena. *Surf. Sci. Rep.* **2008**, *63*, 515–582. [[CrossRef](#)]

15. Wang, H.; Lewis, J.P. Effects of dopant states on photoactivity in carbon-doped TiO₂. *J. Phys. Condens. Matter* **2005**, *17*, L209. [[CrossRef](#)]
16. Xiang, Q.; Yu, J.; Wang, W.; Jaroniec, M. Nitrogen self-doped nanosized TiO₂ sheets with exposed {001} facets for enhanced visible-light photocatalytic activity. *Chem. Commun.* **2011**, *47*, 6906–6908. [[CrossRef](#)]
17. Umebayashi, T.; Yamaki, T.; Tanaka, S.; Asai, K. Visible light-induced degradation of methylene blue on S-doped TiO₂. *Chem. Lett.* **2003**, *32*, 330–331. [[CrossRef](#)]
18. Li, D.; Haneda, H.; Hishita, S.; Ohashi, N. Visible-light-driven N-F-codoped TiO₂ photocatalysts. 2. Optical characterization, photocatalysis, and potential application to air purification. *Chem. Mater.* **2005**, *17*, 2596–2602. [[CrossRef](#)]
19. Asahi, R.; Morikawa, T.; Ohwaki, T.; Aoki, K.; Taga, Y. Visible-light photocatalysis in nitrogen-doped titanium oxides. *Science* **2001**, *293*, 269–271. [[CrossRef](#)]
20. Asahi, R.; Morikawa, T.; Irie, H.; Ohwaki, T. Nitrogen-doped titanium dioxide as visible-light-sensitive photocatalyst: Designs, developments, and prospects. *Chem. Rev.* **2014**, *114*, 9824–9852. [[CrossRef](#)]
21. Nakamura, R.; Tanaka, T.; Nakato, Y. Mechanism for visible light responses in anodic photocurrents at N-doped TiO₂ film electrodes. *J. Phys. Chem. B* **2004**, *108*, 10617–10620. [[CrossRef](#)]
22. Zhang, X.; Liu, A.; Cao, Y.; Xie, J.; Jia, W.; Jia, D. Interstitial N-doped SrSnO₃ perovskite: Structural design, modification and photocatalytic degradation of dyes. *New J. Chem.* **2019**, *43*, 10965–10972. [[CrossRef](#)]
23. Meng, F.; Hong, Z.; Arndt, J.; Li, M.; Zhi, M.; Yang, F.; Wu, N. Visible light photocatalytic activity of nitrogen-doped La₂Ti₂O₇ nanosheets originating from band gap narrowing. *Nano Res.* **2012**, *5*, 213–221. [[CrossRef](#)]
24. Padervand, M.; Ghasemi, S.; Hajiahmadi, S.; Wang, C. K₄Nb₆O₁₇/Fe₃N/α-Fe₂O₃/C₃N₄ as an enhanced visible light-driven quaternary photocatalyst for acetamiprid photodegradation, CO₂ reduction, and cancer cells treatment. *Appl. Surf. Sci.* **2021**, *544*, 148939. [[CrossRef](#)]
25. Rhimi, B.; Padervand, M.; Jouini, H.; Ghasemi, S.; Bahnemann, D.W.; Wang, C. Recent progress in NO_x photocatalytic removal: Surface/interface engineering and mechanistic understanding. *J. Environ. Chem. Eng.* **2022**, *10*, 108566. [[CrossRef](#)]
26. Marschall, R.; Wang, L. Non-metal doping of transition metal oxides for visible-light photocatalysis. *Catal. Today* **2014**, *225*, 111–135. [[CrossRef](#)]
27. Burda, C.; Lou, Y.; Chen, X.; Samia, A.C.; Stout, J.; Gole, J.L. Enhanced nitrogen doping in TiO₂ nanoparticles. *Nano Lett.* **2003**, *3*, 1049–1051. [[CrossRef](#)]
28. Liu, G.; Yin, L.-C.; Wang, J.; Niu, P.; Zhen, C.; Xie, Y.; Cheng, H.-M. A red anatase TiO₂ photocatalyst for solar energy conversion. *Energy Environ. Sci.* **2012**, *5*, 9603–9610. [[CrossRef](#)]
29. Sathish, M.; Viswanathan, B.; Viswanath, R.; Gopinath, C.S. Synthesis, characterization, electronic structure, and photocatalytic activity of nitrogen-doped TiO₂ nanocatalyst. *Chem. Mater.* **2005**, *17*, 6349–6353. [[CrossRef](#)]
30. Kobayakawa, K.; Murakami, Y.; Sato, Y. Visible-light active N-doped TiO₂ prepared by heating of titanium hydroxide and urea. *J. Photochem. Photobiol. A* **2005**, *170*, 177–179. [[CrossRef](#)]
31. Wang, J.; Asakura, Y.; Hasegawa, T.; Yin, S. High-concentration N-doped La₂Ti₂O₇ nanocrystals: Effects of nano-structuration and doping sites on enhancing the photocatalytic activity. *Chem. Eng. J.* **2021**, *423*, 130220. [[CrossRef](#)]
32. Cao, J.; Hasegawa, T.; Asakura, Y.; Sun, P.; Yang, S.; Li, B.; Cao, W.; Yin, S. Synthesis and color tuning of titanium oxide inorganic pigment by phase control and mixed-anion co-doping. *Adv. Powder Technol.* **2022**, *33*, 103576. [[CrossRef](#)]
33. Lu, J.; Zhang, Q.; Wang, J.; Saito, F.; Uchida, M. Synthesis of N-Doped ZnO by grinding and subsequent heating ZnO-urea mixture. *Powder Technol.* **2006**, *162*, 33–37. [[CrossRef](#)]
34. Regmi, C.; Kshetri, Y.K.; Kim, T.-H.; Dhakal, D.; Lee, S.W. Mechanistic understanding of enhanced photocatalytic activity of N-doped BiVO₄ towards degradation of ibuprofen: An experimental and theoretical approach. *Mol. Catal.* **2019**, *470*, 8–18. [[CrossRef](#)]
35. Elghniji, K.; Ksibi, M.; Elaloui, E. Sol–gel reverse micelle preparation and characterization of N-doped TiO₂: Efficient photocatalytic degradation of methylene blue in water under visible light. *J. Ind. Eng. Chem.* **2012**, *18*, 178–182. [[CrossRef](#)]
36. Okato, T.; Sakano, T.; Obara, M. Suppression of photocatalytic efficiency in highly N-doped anatase films. *Phys. Rev. B* **2005**, *72*, 115124. [[CrossRef](#)]
37. Ma, Z.; Wu, K.; Sa, R.; Li, Q.; He, C.; Yi, Z. Mechanism of enhanced photocatalytic activities on N-doped La₂Ti₂O₇: An insight from density-functional calculations. *Int. J. Hydrog. Energy* **2015**, *40*, 980–989. [[CrossRef](#)]
38. Wang, J.; Yin, S.; Komatsu, M.; Zhang, Q.; Saito, F.; Sato, T. Preparation and characterization of nitrogen doped SrTiO₃ photocatalyst. *J. Photochem. Photobiol. A* **2004**, *165*, 149–156. [[CrossRef](#)]
39. Jin, Y.; Li, F.; Cui, P.; Yang, Y.; Ke, Q.; Ha, M.N.; Zhan, W.; Ruan, F.; Wan, C.; Lei, Z. Jahn-Teller distortion assisted interstitial nitrogen engineering: Enhanced oxygen dehydrogenation activity of N-doped Mn_xCo_{3-x}O₄ hierarchical micro-nano particles. *Nano Res.* **2021**, *14*, 2637–2643. [[CrossRef](#)]
40. Fang, Z.; Bueken, B.; De Vos, D.E.; Fischer, R.A. Defect-engineered metal-organic frameworks. *Angew. Chem. Int. Ed.* **2015**, *54*, 7234–7254. [[CrossRef](#)]
41. Kim, M.; Lee, B.; Ju, H.; Kim, J.Y.; Kim, J.; Lee, S.W. Oxygen-vacancy-introduced BaSnO_{3-δ} photoanodes with tunable band structures for efficient solar-driven water splitting. *Adv. Mater.* **2019**, *31*, 1903316. [[CrossRef](#)] [[PubMed](#)]
42. Giannakas, A.; Seristatidou, E.; Deligiannakis, Y.; Konstantinou, I. Photocatalytic activity of N-doped and N-F co-doped TiO₂ and reduction of chromium (VI) in aqueous solution: An EPR study. *Appl. Catal. B* **2013**, *132*, 460–468. [[CrossRef](#)]

43. Di Valentin, C.; Finazzi, E.; Pacchioni, G.; Selloni, A.; Livraghi, S.; Paganini, M.C.; Giamello, E. N-doped TiO₂: Theory and experiment. *Chem. Phys.* **2007**, *339*, 44–56. [[CrossRef](#)]
44. Bai, S.; Zhang, N.; Gao, C.; Xiong, Y. Defect engineering in photocatalytic materials. *Nano Energy* **2018**, *53*, 296–336. [[CrossRef](#)]
45. Gong, X.-Q.; Selloni, A. Reactivity of anatase TiO₂ nanoparticles: The role of the minority (001) surface. *J. Phys. Chem. B* **2005**, *109*, 19560–19562. [[CrossRef](#)]
46. Selloni, A. Anatase shows its reactive side. *Nat. Mater.* **2008**, *7*, 613–615. [[CrossRef](#)]
47. Takata, T.; Pan, C.; Domen, K. Recent progress in oxynitride photocatalysts for visible-light-driven water splitting. *Sci. Technol. Adv. Mater.* **2015**, *16*, 033506. [[CrossRef](#)] [[PubMed](#)]
48. Kageyama, H.; Hayashi, K.; Maeda, K.; Atfield, J.P.; Hiroi, Z.; Rondinelli, J.M.; Poeppelmeier, K.R. Expanding frontiers in materials chemistry and physics with multiple anions. *Nat. Commun.* **2018**, *9*, 772. [[CrossRef](#)] [[PubMed](#)]
49. Hojamberdiev, M.; Yubuta, K.; Vequizo, J.J.M.; Yamakata, A.; Oishi, S.; Domen, K.; Teshima, K. NH₃-assisted flux growth of cube-like BaTaO₂N submicron crystals in a completely ionized nonaqueous high-temperature solution and their water splitting activity. *Cryst. Growth Des.* **2015**, *15*, 4663–4671. [[CrossRef](#)]
50. Asakura, Y.; Nishimura, Y.; Masubuchi, Y.; Yin, S. Utility of ZnGa₂O₄ nanoparticles obtained hydrothermally for preparation of GaN:ZnO solid solution nanoparticles and transparent films. *Eur. J. Inorg. Chem.* **2019**, *2019*, 1999–2005. [[CrossRef](#)]
51. Hermawan, A.; Asakura, Y.; Yin, S. Morphology control of aluminum nitride (AlN) for a novel high-temperature hydrogen sensor. *Int. J. Miner. Metall. Mater.* **2020**, *27*, 1560–1567. [[CrossRef](#)]
52. Maeda, K.; Teramura, K.; Domen, K. Development of cocatalysts for photocatalytic overall water splitting on (Ga_{1-x}Zn_x)(N_{1-x}O_x) solid solution. *Catal. Surv. Asia* **2007**, *11*, 145–157. [[CrossRef](#)]
53. Lee, Y.; Terashima, H.; Shimodaira, Y.; Teramura, K.; Hara, M.; Kobayashi, H.; Domen, K.; Yashima, M. Zinc germanium oxynitride as a photocatalyst for overall water splitting under visible light. *J. Phys. Chem. C* **2007**, *111*, 1042–1048. [[CrossRef](#)]
54. Higashi, M.; Abe, R.; Takata, T.; Domen, K. Photocatalytic overall water splitting under visible light using ATaO₂N (A = Ca, Sr, Ba) and WO₃ in a IO₃⁻/I⁻ shuttle redox mediated system. *Chem. Mater.* **2009**, *21*, 1543–1549. [[CrossRef](#)]
55. Ueda, K.; Kato, H.; Kobayashi, M.; Hara, M.; Kakihana, M. Control of valence band potential and photocatalytic properties of Na_xLa_{1-x}TaO_{1+2x}N_{2-2x} oxynitride solid solutions. *J. Mater. Chem. A* **2013**, *1*, 3667–3674. [[CrossRef](#)]
56. Asakura, Y.; Inaguma, Y.; Ueda, K.; Masubuchi, Y.; Yin, S. Synthesis of gallium oxynitride nanoparticles through hydrothermal reaction in the presence of acetylene black and their photocatalytic NO_x decomposition. *Nanoscale* **2018**, *10*, 1837–1844. [[CrossRef](#)]
57. Lee, K.; Lu, Y.-G.; Chuang, C.-H.; Ciston, J.; Dukovic, G. Synthesis and characterization of (Ga_{1-x}Zn_x)(N_{1-x}O_x) nanocrystals with a wide range of compositions. *J. Mater. Chem. A* **2016**, *4*, 2927–2935. [[CrossRef](#)]
58. Wu, A.; Li, J.; Liu, B.; Yang, W.; Jiang, Y.; Liu, L.; Zhang, X.; Xiong, C.; Jiang, X. Band-gap tailoring and visible-light-driven photocatalytic performance of porous (GaN)_{1-x}(ZnO)_x solid solution. *Dalton Trans.* **2017**, *46*, 2643–2652. [[CrossRef](#)]
59. Sun, X.; Maeda, K.; Le Faucheur, M.; Teramura, K.; Domen, K. Preparation of (Ga_{1-x}Zn_x)(N_{1-x}O_x) solid-solution from ZnGa₂O₄ and ZnO as a photo-catalyst for overall water splitting under visible light. *Appl. Catal. A* **2007**, *327*, 114–121. [[CrossRef](#)]
60. Wang, J.; Asakura, Y.; Yin, S. Preparation of (Zn_{1+x}Ge)(N₂O_x) nanoparticles with enhanced NO_x decomposition activity under visible light irradiation by nitridation of Zn₂GeO₄ nanoparticles designed precisely. *Nanoscale* **2019**, *11*, 20151–20160. [[CrossRef](#)]
61. Xiong, F.Q.; Wan, L.; Li, Y.; Thomas, T.; DiSalvo, F.J.; Yang, M. Crucial Role of Donor Density in the Performance of Oxynitride Perovskite LaTiO₂N for Photocatalytic Water Oxidation. *ChemSusChem* **2017**, *10*, 930–937. [[CrossRef](#)]
62. Higashi, M.; Domen, K.; Abe, R. Fabrication of an efficient BaTaO₂N photoanode harvesting a wide range of visible light for water splitting. *J. Am. Chem. Soc.* **2013**, *135*, 10238–10241. [[CrossRef](#)]
63. Knez, M.; Scholz, R.; Nielsch, K.; Pippel, E.; Hesse, D.; Zacharias, M.; Gösele, U. Monocrystalline spinel nanotube fabrication based on the Kirkendall effect. *Nat. Mater.* **2006**, *5*, 627–631.
64. Solís, R.R.; Bedia, J.; Rodríguez, J.J.; Belver, C. A review on alkaline earth metal titanates for applications in photocatalytic water purification. *Chem. Eng. J.* **2021**, *409*, 128110.
65. Hwang, D.W.; Kim, H.G.; Lee, J.S.; Kim, J.; Li, W.; Oh, S.H. Photocatalytic hydrogen production from water over M-doped La₂Ti₂O₇ (M = Cr, Fe) under visible light irradiation (λ > 420 nm). *J. Phys. Chem. B* **2005**, *109*, 2093–2102.
66. Wang, Z.; Teramura, K.; Hosokawa, S.; Tanaka, T. Photocatalytic conversion of CO₂ in water over Ag-modified La₂Ti₂O₇. *Appl. Catal. B* **2015**, *163*, 241–247. [[CrossRef](#)]
67. Izawa, C.; Watanabe, T. Direct fabrication of La₂Ti₂O₇ films on titanium metal substrate by hydrothermal reaction. *Trans. Mater. Res. Soc. Japan* **2011**, *36*, 413–416. [[CrossRef](#)]
68. Wang, R.; Xu, D.; Liu, J.; Li, K.; Wang, H. Preparation and photocatalytic properties of CdS/La₂Ti₂O₇ nanocomposites under visible light. *Chem. Eng. J.* **2011**, *168*, 455–460. [[CrossRef](#)]
69. Hojamberdiev, M.; Yamaguchi, A.; Yubuta, K.; Oishi, S.; Teshima, K. Fabrication of La₂Ti₂O₇ crystals using an alkali-metal molybdate flux growth method and their nitridability to form LaTiO₂N crystals under a high-temperature NH₃ atmosphere. *Inorg. Chem.* **2015**, *54*, 3237–3244. [[CrossRef](#)]
70. Onozuka, K.; Kawakami, Y.; Imai, H.; Yokoi, T.; Tatsumi, T.; Kondo, J. Perovskite-type La₂Ti₂O₇ mesoporous photocatalyst. *J. Solid State Chem.* **2012**, *192*, 87–92. [[CrossRef](#)]
71. Li, Y.; Xu, M.; Yan, X.; Addiego, C.; Jiang, L.; Wang, H.; Zhu, J. Origin of the enhanced piezoelectricity of vanadium-doped La₂Ti₂O₇ ceramics. *J. Phys. Chem. C* **2021**, *125*, 26180–26187. [[CrossRef](#)]

72. Meng, F.; Li, J.; Hong, Z.; Zhi, M.; Sakla, A.; Xiang, C.; Wu, N. Photocatalytic generation of hydrogen with visible-light nitrogen-doped lanthanum titanium oxides. *Catal. Today* **2013**, *199*, 48–52. [[CrossRef](#)]
73. Cai, X.; Zhang, J.; Fujitsuka, M.; Majima, T. Graphitic-C₃N₄ hybridized N-doped La₂Ti₂O₇ two-dimensional layered composites as efficient visible-light-driven photocatalyst. *Appl. Catal. B* **2017**, *202*, 191–198. [[CrossRef](#)]
74. Wang, J.; Tafen, D.N.; Lewis, J.P.; Hong, Z.; Manivannan, A.; Zhi, M.; Li, M.; Wu, N. Origin of photocatalytic activity of nitrogen-doped TiO₂ nanobelts. *J. Am. Chem. Soc.* **2009**, *131*, 12290–12297.
75. Wan, S.; Qi, F.; Jin, W.; Guo, X.; Liu, H.; Zhao, J.; Zhang, J.; Tang, C. Construction of ultrafine Ag₃PO₄ nanoparticle and La₂Ti₂O₇ nanosheet 0D/2D heterojunctions with improved photocatalytic performance. *J. Alloys Compd.* **2018**, *740*, 901–909. [[CrossRef](#)]
76. Ao, Y.; Wang, K.; Wang, P.; Wang, C.; Hou, J. Synthesis of novel 2D-2D pn heterojunction BiOBr/La₂Ti₂O₇ composite photocatalyst with enhanced photocatalytic performance under both UV and visible light irradiation. *Appl. Catal. B* **2016**, *194*, 157–168. [[CrossRef](#)]
77. Wang, K.; Jiang, L.; Wu, X.; Zhang, G. Vacancy mediated Z-scheme charge transfer in a 2D/2D La₂Ti₂O₇/g-C₃N₄ nanojunction as a bifunctional photocatalyst for solar-to-energy conversion. *J. Mater. Chem. A* **2020**, *8*, 13241–13247.
78. Shiraishi, Y.; Shiota, S.; Hirakawa, H.; Tanaka, S.; Ichikawa, S.; Hirai, T. Titanium dioxide/reduced graphene oxide hybrid photocatalysts for efficient and selective partial oxidation of cyclohexane. *ACS Catal.* **2017**, *7*, 293–300. [[CrossRef](#)]
79. Ren, L.; Yi, X.; Tong, L.; Zhou, W.; Wang, D.; Liu, L.; Ye, J. Nitrogen-doped ultrathin graphene encapsulated Cu nanoparticles decorated on SrTiO₃ as an efficient water oxidation photocatalyst with activity comparable to BiVO₄ under visible-light irradiation. *Appl. Catal. B* **2020**, *279*, 119352. [[CrossRef](#)]
80. Xing, Z.; Ju, Z.; Zhao, Y.; Wan, J.; Zhu, Y.; Qiang, Y.; Qian, Y. One-pot hydrothermal synthesis of Nitrogen-doped graphene as high-performance anode materials for lithium ion batteries. *Sci. Rep.* **2016**, *6*, 26146.
81. Hua, Z.; Zhang, X.; Bai, X.; Lv, L.; Ye, Z.; Huang, X. Nitrogen-doped perovskite-type La₂Ti₂O₇ decorated on graphene composites exhibiting efficient photocatalytic activity toward bisphenol A in water. *J. Colloid Interface Sci.* **2015**, *450*, 45–53. [[CrossRef](#)] [[PubMed](#)]
82. Meng, F.; Cushing, S.K.; Li, J.; Hao, S.; Wu, N. Enhancement of solar hydrogen generation by synergistic interaction of La₂Ti₂O₇ photocatalyst with plasmonic gold nanoparticles and reduced graphene oxide nanosheets. *ACS Catal.* **2015**, *5*, 1949–1955. [[CrossRef](#)]
83. Ge, L.; Han, C.; Liu, J. Novel visible light-induced g-C₃N₄/Bi₂WO₆ composite photocatalysts for efficient degradation of methyl orange. *Appl. Catal. B* **2011**, *108*, 100–107.
84. Xia, M.; Yan, X.; Li, H.; Wells, N.; Yang, G. Well-designed efficient charge separation in 2D/2D N doped La₂Ti₂O₇/ZnIn₂S₄ heterojunction through band structure/morphology regulation synergistic effect. *Nano Energy* **2020**, *78*, 105401.
85. Moriya, Y.; Takata, T.; Domen, K. Recent progress in the development of (oxy) nitride photocatalysts for water splitting under visible-light irradiation. *Coord. Chem. Rev.* **2013**, *257*, 1957–1969. [[CrossRef](#)]
86. Kasahara, A.; Nukumizu, K.; Hitoki, G.; Takata, T.; Kondo, J.N.; Hara, M.; Kobayashi, H.; Domen, K. Photoreactions on LaTiO₂N under visible light irradiation. *J. Phys. Chem. A* **2002**, *106*, 6750–6753. [[CrossRef](#)]
87. Zhang, F.; Yamakata, A.; Maeda, K.; Moriya, Y.; Takata, T.; Kubota, J.; Teshima, K.; Oishi, S.; Domen, K. Cobalt-modified porous single-crystalline LaTiO₂N for highly efficient water oxidation under visible light. *J. Am. Chem. Soc.* **2012**, *134*, 8348–8351. [[CrossRef](#)]
88. Maegli, A.E.; Pokrant, S.; Hisatomi, T.; Trottmann, M.; Domen, K.; Weidenkaff, A. Enhancement of photocatalytic water oxidation by the morphological control of LaTiO₂N and cobalt oxide catalysts. *J. Phys. Chem. C* **2013**, *118*, 16344–16351. [[CrossRef](#)]
89. Matsukawa, M.; Ishikawa, R.; Hisatomi, T.; Moriya, Y.; Shibata, N.; Kubota, J.; Ikuhara, Y.; Domen, K. Enhancing photocatalytic activity of LaTiO₂N by removal of surface reconstruction layer. *Nano Lett.* **2014**, *14*, 1038–1041. [[CrossRef](#)]
90. Li, Y.; Cheng, X.; Ruan, X.; Song, H.; Lou, Z.; Ye, Z.; Zhu, L. Enhancing photocatalytic activity for visible-light-driven H₂ generation with the surface reconstructed LaTiO₂N nanostructures. *Nano Energy* **2015**, *12*, 775–784. [[CrossRef](#)]
91. Inoue, Y. Photocatalytic water splitting by RuO₂-loaded metal oxides and nitrides with d⁰- and d¹⁰-related electronic configurations. *Energy Environ. Sci.* **2009**, *2*, 364–386.
92. Hu, J.; Song, E.; Ye, S.; Zhou, B.; Zhang, Q. Anomalous spontaneous-reduction of Mn⁷⁺/Mn⁴⁺ to Mn²⁺ and luminescence properties in Zn₂GeO₄:Mn. *J. Mater. Chem. C* **2017**, *5*, 3343–3351. [[CrossRef](#)]
93. Huang, J.; Ding, K.; Hou, Y.; Wang, X.; Fu, X. Synthesis and photocatalytic activity of Zn₂GeO₄ nanorods for the degradation of organic pollutants in water. *ChemSusChem* **2008**, *1*, 1011–1019. [[CrossRef](#)] [[PubMed](#)]
94. Ma, B.; Wen, F.; Jiang, H.; Yang, J.; Ying, P.; Li, C. The synergistic effects of two co-catalysts on Zn₂GeO₄ on photocatalytic water splitting. *Catal. Lett.* **2010**, *134*, 78–86. [[CrossRef](#)]
95. Feng, Y.; Li, X.; Shao, Z.; Wang, H. Morphology-dependent performance of Zn₂GeO₄ as a high-performance anode material for rechargeable lithium ion batteries. *J. Mater. Chem. A* **2015**, *3*, 15274–15279. [[CrossRef](#)]
96. Wu, S.; Wang, Z.; Ouyang, X.; Lin, Z. Core-shell Zn₂GeO₄ nanorods and their size-dependent photoluminescence properties. *Nanoscale* **2013**, *5*, 12335–12341. [[CrossRef](#)]
97. Yi, R.; Feng, J.; Lv, D.; Gordin, M.L.; Chen, S.; Choi, D.; Wang, D. Amorphous Zn₂GeO₄ nanoparticles as anodes with high reversible capacity and long cycling life for Li-ion batteries. *Nano Energy* **2013**, *2*, 498–504. [[CrossRef](#)]

98. Yan, S.; Wan, L.; Li, Z.; Zou, Z. Facile temperature-controlled synthesis of hexagonal Zn_2GeO_4 nanorods with different aspect ratios toward improved photocatalytic activity for overall water splitting and photoreduction of CO_2 . *Chem. Commun.* **2011**, *47*, 5632–5634. [[CrossRef](#)]
99. Boppana, V.B.R.; Hould, N.D.; Lobo, R.F. Synthesis, characterization and photocatalytic properties of novel zinc germanate nano-materials. *J. Solid State Chem.* **2011**, *184*, 1054–1062.
100. Yan, S.; Wang, J.; Zou, Z. An anion-controlled crystal growth route to Zn_2GeO_4 nanorods for efficient photocatalytic conversion of CO_2 into CH_4 . *Dalton Trans.* **2013**, *42*, 12975–12979. [[CrossRef](#)]
101. Lu, Y.; Jin, R.; Qiao, Y.; Liu, W.; Wang, K.; Wang, X.; Wang, C. Preparation of self-assembled N- Zn_2GeO_4 nanocomposite and their photocatalytic properties. *Int. J. Electrochem. Sci* **2020**, *15*, 10243–10252. [[CrossRef](#)]
102. Lan, N.; Tuan, D.; Tuan, T.; Kien, N.; Thang, C.; Tung, N.; Giang, N. Effect of Nitrogen Doping on the Structural and Optical Properties of Zn_2GeO_4 Phosphors. *J. Appl. Spectrosc.* **2022**, *89*, 652–657.
103. Yang, K.; Dai, Y.; Huang, B. Study of the nitrogen concentration influence on N-doped TiO_2 anatase from first-principles calculations. *J. Phys. Chem. C* **2007**, *111*, 12086–12090. [[CrossRef](#)]
104. Di Valentin, C.; Finazzi, E.; Pacchioni, G.; Selloni, A.; Livraghi, S.; Czoska, A.; Paganini, M.; Giamello, E. Density functional theory and electron paramagnetic resonance study on the effect of N – F codoping of TiO_2 . *Chem. Mater.* **2008**, *20*, 3706–3714. [[CrossRef](#)]
105. Li, Y.; Ding, K.; Cheng, B.; Zhang, Y.; Lu, Y. N, F-monodoping and N/F-codoping effects on the electronic structures and optical performances of Zn_2GeO_4 . *Phys. Chem. Chem. Phys.* **2015**, *17*, 5613–5623.
106. Lee, Y.; Teramura, K.; Hara, M.; Domen, K. Modification of $(Zn_{1+x}Ge)(N_2O_x)$ solid solution as a visible light driven photocatalyst for overall water splitting. *Chem. Mater.* **2007**, *19*, 2120–2127. [[CrossRef](#)]
107. Wang, J.; Asakura, Y.; Yin, S. Synthesis of zinc germanium oxynitride nanotube as a visible-light driven photocatalyst for NO_x decomposition through ordered morphological transformation from Zn_2GeO_4 nanorod obtained by hydrothermal reaction. *J. Hazard. Mater.* **2020**, *396*, 122709. [[CrossRef](#)]
108. Sato, J.; Kobayashi, H.; Ikarashi, K.; Saito, N.; Nishiyama, H.; Inoue, Y. Photocatalytic activity for water decomposition of RuO_2 -dispersed Zn_2GeO_4 with d^{10} configuration. *J. Phys. Chem. B* **2004**, *108*, 4369–4375. [[CrossRef](#)]
109. Yang, M.; Ji, Y.; Liu, W.; Wang, Y.; Liu, X. Facile microwave-assisted synthesis and effective photocatalytic hydrogen generation of Zn_2GeO_4 with different morphology. *RSC Adv.* **2014**, *4*, 15048–15054. [[CrossRef](#)]
110. Liu, Q.; Zhou, Y.; Kou, J.; Chen, X.; Tian, Z.; Gao, J.; Yan, S.; Zou, Z. High-yield synthesis of ultralong and ultrathin Zn_2GeO_4 nanoribbons toward improved photocatalytic reduction of CO_2 into renewable hydrocarbon fuel. *J. Am. Chem. Soc.* **2010**, *132*, 14385–14387. [[CrossRef](#)]
111. Yu, L.; Zou, R.; Zhang, Z.; Song, G.; Chen, Z.; Yang, J.; Hu, J. A Zn_2GeO_4 -ethylenediamine hybrid nanoribbon membrane as a recyclable adsorbent for the highly efficient removal of heavy metals from contaminated water. *Chem. Commun.* **2011**, *47*, 10719–10721. [[CrossRef](#)] [[PubMed](#)]
112. Zhang, N.; Ouyang, S.; Li, P.; Zhang, Y.; Xi, G.; Kako, T.; Ye, J. Ion-exchange synthesis of a micro/mesoporous Zn_2GeO_4 photocatalyst at room temperature for photoreduction of CO_2 . *Chem. Commun.* **2011**, *47*, 2041–2043. [[CrossRef](#)] [[PubMed](#)]
113. Liu, Q.; Zhou, Y.; Tian, Z.; Chen, X.; Gao, J.; Zou, Z. Zn_2GeO_4 crystal splitting toward sheaf-like, hyperbranched nanostructures and photocatalytic reduction of CO_2 into CH_4 under visible light after nitridation. *J. Mater. Chem.* **2012**, *22*, 2033–2038. [[CrossRef](#)]
114. Chen, H.; Yu, G.; Li, G.D.; Xie, T.; Sun, Y.; Liu, J.; Li, H.; Huang, X.; Wang, D.; Asefa, T. Unique electronic structure in a porous Ga-In bimetallic oxide nano-photocatalyst with atomically thin pore walls. *Angew. Chem. Int. Ed.* **2016**, *55*, 11442–11446. [[CrossRef](#)] [[PubMed](#)]